IEEE Access
Multidisciplinary ⋮ Rapid Review ⋮ Open Access Journal

Received April 8, 2022, accepted April 17, 2022, date of publication April 22, 2022, date of current version April 29, 2022.

Digital Object Identifier 10.1109/ACCESS.2022.3169414

Efficiency Enhancement of GaAs Nano Solar Cell Based on 2D Photonic Crystal Trapping Layer and 2D Index Modulation Layer

MORSY A. MORSY AND KHALID SALEH
Department of Electrical Engineering, College of Engineering, Shaqra University, Al Dawadmi, Riyadh 11911, Saudi Arabia
Corresponding author: Morsy A. Morsy (morsy_ismail@su.edu.sa)

This work was supported by the Deputyship for Research & Innovation, Ministry of Education, Saudi Arabia, under Project IFP2021-055.

ABSTRACT In this paper, a nano solar cell structure based on a two-dimensional photonic crystal (2D-PhC) antireflection coating (ARC) trapping layer and a 2D- graded-index (2D-GI) GaAs active layer is presented. These components improve the solar absorption, in-coupling efficiency, quantum efficiency, and optical properties of the active layer. The proposed cell absorption and conversion efficiency were analyzed as a function of the cell layer thickness in comparison with the Lambertian absorption and cell efficiency limits. Additionally, each layer thickness was optimized to enhance the overall solar efficiency. All simulations were conducted in the 300 to 1100 nm range using finite difference time domain (FDTD) analysis, where the 2D-PhC structure was represented by indium tin oxide (ITO) nanorods in an air background. In addition, p-Al(0.85)GaAs/n-Al(0.35)GaAs two-window confinement layers are utilized in contact with the 907-nm GaAs active layer as a perfect match with the 1840-nm ITO-ARC layer to improve the confinement efficiency. Moreover, p-Al(0.85)GaAs/GaAs and GaAs/n-Al(0.35)GaAs 2D-GI active layer structures are used for index modulation to enhance the active layer properties and increase the cell short-circuit current. The main objective of this study is to determine the optimum design of a solar cell that can provide the highest power conversion efficiency using inexpensive semiconductor materials. One of the expected results from this research is the design of a 100-μm^2 nano solar cell with 39.2% conversion efficiency, a short circuit current density of 44.38 mA/cm^2, and an open-circuit voltage of 1 V.

INDEX TERMS Two-dimensional photonic crystal (2D-PhC), light trapping, 2D-index modulation, absorption, conversion efficiency, short circuit current, open circuit voltage.

I. INTRODUCTION

Because of the increase in human consumption of energy, it has become necessary to search for sources of energy that are renewable, safe, clean, and inexpensive. Solar energy is the best candidate for this purpose. Many attempts have been made to design the best and least expensive structures for generating solar energy. Nanostructures have been widely applied to solar cells, as they demonstrate promising features for future high-efficiency and low-cost applications. Compared with conventional solar cells, nanocrystal solar cells have the advantages of producing energy with higher efficiency, higher electrical storage capacity, and lower pollution. There are many techniques for implementing nanocrystal solar cells [1]–[14]. One of these techniques is based on reducing material usage by utilizing thin-film crystalline silicon or GaAs solar cells with light-trapping structures, which has the advantage of enhancing the light absorption within the semiconductor absorber/active layer. Effective light-trapping structures have various design considerations studying the effect of these structures on the cell efficiency versus the active layer thickness [1]–[10]. Other techniques implement perovskite solar cells using organic/inorganic active layer for efficiency enhancement and studying the radio frequency performance of GaAs material [11]–[14]. Reducing light reflection on the surface of solar cells is a key factor in increasing the amount of light absorption, and hence, the conversion efficiency. The values of the refractive indices of the materials used in the manufacture of solar cells play a major role in controlling the light reflections at the interface surface between the cell and air. Therefore, an antireflection coating (ARC)

The associate editor coordinating the review of this manuscript and approving it for publication was Zhongyi Guo.

and/or specific surface texture can be used with crystalline silicon or GaAs solar cells to achieve a lower amount of light reflection, thereby increasing the absorbed optical power [15]–[22]. The heterojunction technique is also used to enhance the carrier confinement inside the cell active layer, thereby increasing the amount of photocurrent [23]–[27]. Recently, various solutions have been developed with the aim of reducing the amount of reflection and consequently increasing the conversion efficiency of solar cells. Almost all of these solutions are related to two-dimensional photonic crystal (2D-PhC) technology. Such solutions depend on the addition of a thin-film layer on the surface of the cell. This layer aims to increase the rate of cell light absorption by modulating the refractive index of the dielectric material used in this layer. Such layers are usually designed in the form of two-dimensional (2D) periodic structures of dielectric pairs, pyramids, skewed nanorods, hollow spheres, or parts of a sphere [28]–[33]. In other studies that aimed to improve solar efficiency, the effect of the doping concentration in the active layer of the cell on the energy bandgap structure has been analyzed. The main goal of these studies is to examine the effect of extending the absorption wavelength range of silicon materials on increasing photocurrent and solar efficiency. The effect of the thicknesses of the cell active layer and ARC layers has also been studied to investigate the impact of the thicknesses on solar conversion efficiency [1]–[6] and [34]–[42]. Nanotechnology can also be utilized to improve the optical and electrical properties of dielectric materials to improve their characteristics before using them in any application. In addition, studying the energy band gap of nanomaterials is important to determine the effect of the doping concentration in these materials on the absorption rate of light. This knowledge can be used to increase the rate of light absorption by nanomaterials at wavelengths far from the visible light range, thereby increasing the amount of light energy absorbed [15]–[38]. All studies that have been conducted in the literature have this in common: they address the problem of increasing the conversion efficiency of solar cells. Theoretically, the efficiency of a conventional solar cell cannot exceed 33.5%.

The main objective of this research is to provide solutions to improve cell efficiency. This can be done by the following:

- Optimizing the thin-film 2D-PhC structure using an indium tin oxide (ITO)-ARC nanorod trapping layer to reduce the reflection loss, enhancing the light path to exceed the Lambertian absorption limit, and hence increase the cell efficiency.
- Optimizing the heterojunction structure to improve the quantum efficiency of the cells.
- Improving the active layer optical properties using in-contact front and back 2D-graded index (2D-GI) layers to extend the cell visibility wavelength range and consequently increase the cell photocurrent.

To begin the analysis and attain the goal of this study, we will consider the Lambertian efficiency and GaAs single-pass efficiency limits as two references to compare the results of each solution. Fig. 1 illustrates the Lambertian light-trapping efficiency compared with the single-pass GaAs efficiency without any trapping structure with respect to the active layer thickness, ignoring any type of loss [1].

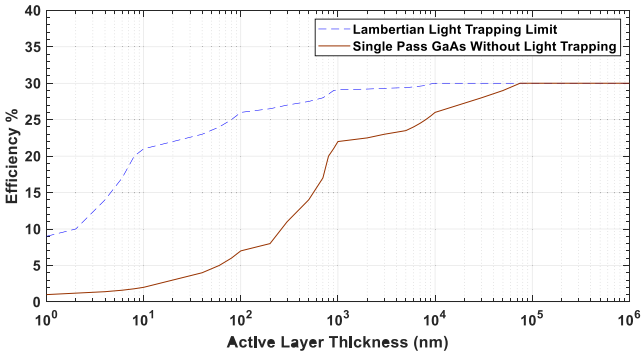

FIGURE 1. GaAs cell efficiency and Lambertian efficiency limit versus active layer thickness using AM1.5G solar spectrum.

In this study, the analysis and optimization of a light-trapping structure based on a nanorod ITO 2D-PhC structure at the top front of a 1-μm GaAs active layer through a p-Al(0.85)GaAs window confinement layer are performed. The active layer is followed by an n-Al(0.35)GaAs window confinement layer and an Al layer as the back reflector electrode to support the top trapping structure [1]. Additionally, to increase the carrier confinement and photocurrent, two 2D-GI layers were employed at the front and back surfaces of the active layer. 2D-GI Index modulation makes the light paths smooth at the layer interface leading to minimum reflections compared with the step-index variations between layers. There are several advantages of using PhC structures, such as perfect index matching between layers, improvement of cell absorption through the solar spectrum, and enhancement of the incident light coupling.

Finite-difference time-domain (FDTD) analysis was used to optimize the cell layers' dimensions to achieve optimum absorption and cell conversion efficiency. GaAs is a direct bandgap material with a high absorption coefficient for the wavelength range from 300 nm to 880 nm. Above this range, the absorption reaches zero [1]. All simulations have been conducted for the wavelength range from 300 nm to 1100 nm to ensure the above statement and show the extension in absorption range due to the uses of the index modulation layers that contact the GaAs active layer. Also, to observe the absorption enhancement due to the use of the ITO trapping layer at the front surface of GaAs Active layer. Such enhancement is due to the impedance matching between the medium of incidence and the confinement layer.

II. LITERATURE REVIEW

Figures that are meant to appear in color, or shades of black/gray. Such figures may include photographs, illustrations, multicolor graphs, and flowcharts

In [1]–[10], the authors introduce different solutions for the cell absorption and efficiency enhancement using a photonic

crystal structure or plasmonic surface for light trapping in GaAs and silicon active layer or p-i-n superlattice based InGaN/GaN. The important result in these research papers is the contribution of the light-trapping structures to the active layer thickness and efficiency. In [11]–[14], authors proved new organic, inorganic, and hybrid inorganic-organic inverted cells with a barrier layer and active organic active layer for efficiency and reliability enhancement. Also, the authors demonstrate a carrier collection mechanism using a hole-collection treated graphene layer. In [15]–[28], a direct numerical solution of Maxwell's equations and drift-diffusion equations were used to develop crystalline-silicon photonic crystal (PhC) solar cells with conversion efficiencies in the range of 29% to 30%. Other techniques have been developed to achieve a conversion efficiency of 33.5%. These techniques are based on using an optimized doped structure to extend the absorption wavelength range up to 1200 nm. This wavelength is too much above the bandgap wavelength, but the authors extend the simulation wavelength to observe the effect of doping on the absorption range. In [29]–[38], perovskite solar cells were developed consisting of a 2D-PhC nano-disk array, which was fabricated using nanosphere lithography. The results show that the output photocurrent has low stability, and the conversion efficiency is only 19%. In [39]–[47], a dielectric film was applied with an anti-reflection coating sub-wavelength structure to fabricate a thin-film silicon solar cell and enhance the in-coupling efficiency at the front surface. The results showed that the short-circuit current is in the range of 29.1 to 30.4 mA/cm^2, and the conversion efficiency is approximately 9.9%. In [48]–[52], some researchers used dye-sensitized nanocrystalline solar cells, whereas others used quantum dots with the same solar cells. In all of these studies, a nanostructured TiO_2 film with visible light-absorbing dyes was utilized to develop solar cells with conversion efficiencies greater than 10%. Consequently, in [53], a porphyrin-sensitized solar cell with cobalt (II/III) was used to develop solar cells with a 12.3% conversion efficiency. In [54]–[66], various loss mechanisms in crystalline solar cells were reported. These losses include the following: 1) reflection loss resulting from the shiny surface of the cell, 2) loss caused by the mismatch between the band-gap energy of the material and the incident photon energy; 3) weak absorption of long-wavelength photons; 4) reduction in photocurrent as a result of Auger recombination; and 5) defects in the semiconductor crystal lattice surface, which also reduces the photocurrent generated by the recombination of electron-hole pairs at the lattice surface. In these studies, many methods have been developed to reduce these losses. However, the results indicated that the conversion efficiency of the developed methods was only 19.1%. In [67]–[75], thin-film crystalline silicon solar cells with light-trapping structures were demonstrated to enhance light absorption within the absorber layer. The trapping layer was an inverted nanopyramid periodic structure fabricated on a low-cost wafer. The designed solar cell produces a current density of 37.5 mA/cm^2 at the highest quantum efficiency

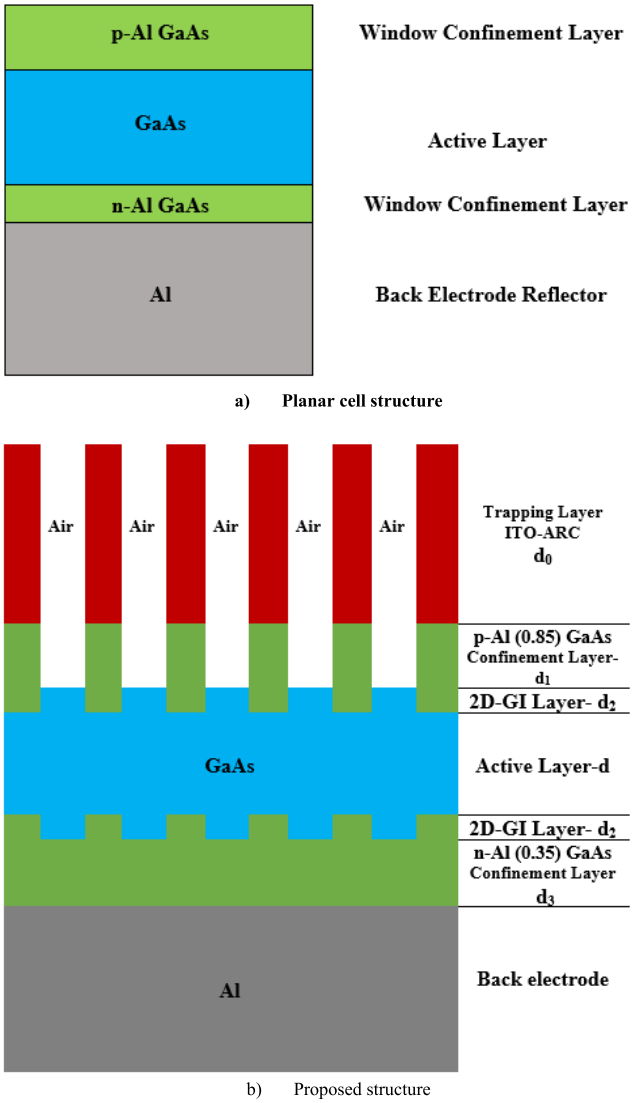

FIGURE 2. Nano solar structure based on 1-μm GaAs active layer: (a) planar reference cell structure and (b) proposed cell structure.

of 100%. The third generation of solar cells is based on nanotechnology and has been developed in [76]–[82]. In this generation, quantum dots and nanoporous materials were used. The developed solar cells in the market that use the InAs/GaAs heterojunction system have conversion efficiencies in the range of 24.6%. In [72]–[82], many trials were conducted to produce stable quantum dot solar cells with enhanced efficiency.

III. METHODOLOGY AND ANALYSIS

A trapping layer consisting of a periodic nanorod 2D-PhC structure using ITO was designed and optimized to enhance cell absorption using FDTD analysis. The design process considers the optimization of the light in-coupling parameters. Fig. 2 (a) and (b) show the planar cell structure with the same thickness as the reference and the proposed cell structure, respectively. Sunlight was assumed to be incident perpendicular to the top ITO 2D-PhC structure. The ITO

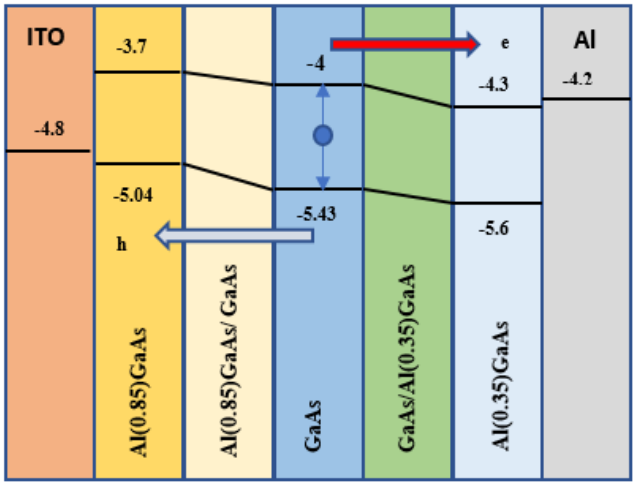

FIGURE 3. Energy band diagram of the proposed structure ITO ARC/p-Al(0.85)GaAs/GaAs/n-Al(0.35)GaAs/Al.

2D-PhC structure has a square lattice for simplicity and consists of nanorod ITO in an air background [83]. This ITO is followed by a p-Al(0.85)GaAs window confinement layer. The active layer is an intermediate layer between this layer and the other n-Al(0.35)GaAs window confinement layer, followed by the Al back electrode reflector. Additionally, the active layer is supported by two front and back 2D-GI layers working as index modulation layers to increase the cell photocurrent. It's known that the index modulation technique is used to reduce the light reflection and increase the light confinement that supports the matching between layers to reach the ideal matching condition. Additionally, to prevent reflection at the top, the ITO refractive index is designed to be a square product of the p-Al(0.85)GaAs and air refractive indices, which is the condition for matching between layers. The first step in the design is the calculation of the ITO periodicity, which represents the lattice constant a and nanorod diameter D. In the FDTD simulation, the cell absorption is used as the cell reference enhancement parameter to obtain the optimum dimensions of the cell layers. The 2D-PhC periodic permittivity is represented by Fourier harmonics, and Maxwell's equations are solved in the frequency domain. In addition, during the simulation, it is assumed that the boundary conditions are periodic in the x-y plane and there is a perfect matching layer in the z-direction.

Figure 3 presents the relevant energy band diagram and electron-hole transportation mechanism. This figure illustrates that the two index modulation layers have a gradual band level that supports the electron-hole transportation and diffusion from the active layer to the confinement layers.

All simulation results are compared with the solar cell Lambertian limits, which were derived with the following assumptions [18], [19]: a) neglecting intrinsic losses, the cell is Lambertian scattered at the front or at the back surfaces when the light is isotropically distributed at each energy level, b) the wavelength inside the active layer is much smaller than the layer thickness, λ/n, making it suitable for

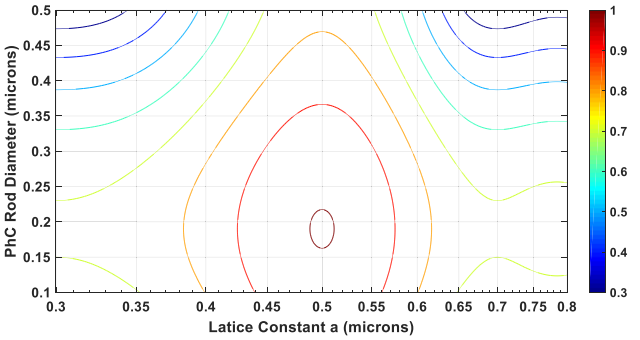

FIGURE 4. Contour map of the cell normalized absorption with respect to the lattice constant a and nanorod diameter D.

ray optics analysis, and c) the GaAs active region shows insufficient absorption through the solar spectrum. This can be represented by the following condition:

$$4n^2\alpha d \ll 1 \tag{1}$$

where, n is the active-layer refractive index, α is the absorption coefficient, and d is the active layer thickness. Using the same assumptions, the absorption can be expressed as a function of $\alpha(\lambda)d_{eff}$, where d_{eff} represents the photon effective pass length through the active layer. At this point, we can express the single pass absorption of the planar cell as

$$A_{single}(\lambda) = 1 - e^{-\alpha(\lambda)\mathrm{d}} \tag{2}$$

Using assumption number three, the maximum absorption of the planar cell assuming an isotropic surrounding medium can be expressed as

$$A_{LL}(\lambda) = 1 - e^{-4n^2\alpha(\lambda)\mathrm{d}} \tag{3}$$

In the proposed cell structure, we can define the total modified cell absorption as the sum of the layer absorption through the cell, which can be expressed as

$$A_{modified}(\lambda) = \sum\nolimits_i A_i(\lambda) \tag{4}$$

where, $A_i(\lambda)$ is the absorption spectrum in each layer of the proposed cell. In addition, the cell absorption enhancement factor $F(\lambda)$ at a certain wavelength λ can be expressed as

$$F(\lambda) = \frac{A_{modified}(\lambda)}{A_{single}(\lambda)} \tag{5}$$

Figure 4 shows the contour map of the cell absorption as a function of the lattice constant a and nanorod diameter D of the ITO trapping structure. The result indicates that the optimum lattice constant is 500 nm and the optimum nanorod diameter is 190 nm, which represents the center point of the smallest contour in Fig.3. When the photon energy exceeds the band gap energy at 0^0 K, each photon can produce an electron hole pair, which is the condition of maximum

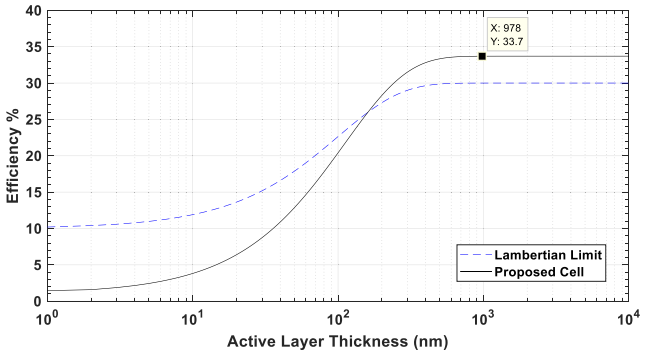

FIGURE 5. Proposed cell efficiency and Lambertian efficiency limit versus the active layer thickness.

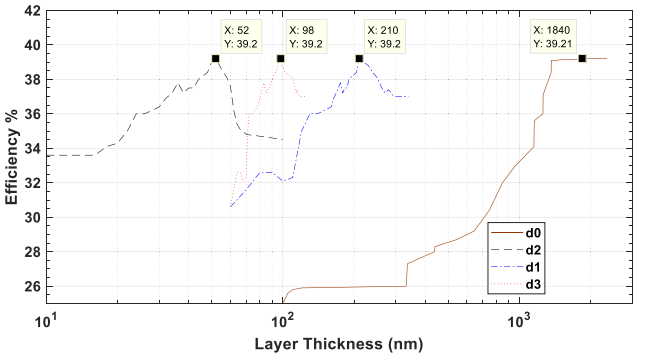

FIGURE 6. Proposed cell efficiency versus thickness for ITO-ARC, p-Al(0.85)GaAs, n-Al(0.35)GaAs, and 2D-GI layers.

efficiency and can be written as:

$$\eta = \frac{\int_0^{\lambda_g} I(\lambda) A(\lambda) \frac{\lambda}{\lambda_g} d\lambda}{\int_0^{\infty} I(\lambda) A(\lambda) d\lambda} \tag{6}$$

where, λ_g is the band gap wavelength, $I(\lambda)$ is the AM1.5G solar spectrum and $A(\lambda)$ is the cell absorption [84]. Using the results in Fig. 4, we can calculate the ultimate cell efficiency as a function of the active layer thickness d. Fig. 5 shows the proposed cell efficiency and the Lambertian efficiency limit versus the active layer thickness. This figure indicates that when the active layer thickness is less than 170 nm, the Lambertian efficiency outperforms the proposed cell efficiency; when the thickness exceeds this value, the proposed cell efficiency surpasses the Lambertian limit and reaches the optimum efficiency of 33.7% at an active layer thickness of 978 nm, including the GI layer thickness. In these calculations, the ITO trapping layer thickness is assumed to be 2 μm, which is approximately twice the active layer thickness.

Maxwell's equations and semiconductor drift diffusion equations were used to improve the optical properties of the active layer and confinement layers and evaluate their characteristics using FDTD simulation tools. In our simulation, we assume that the cell quantum efficiency is unity, and the shadowing coupling efficiencies product $\eta_s \eta_c = 6.6\%$ [22]. The confinement factor and photocurrent are important parameters in the operating wavelength range of 300 to 1100 nm. Therefore, the main objective of this task was to enhance the cell efficiency by optimizing the thickness of each layer. The first step is the optimization of the ITO layer thickness: assuming $d = 978$ nm, $d_1 = 0.2d$, $d_2 = 0.05d$, and $d_3 = 0.1d$, the proposed cell efficiency reaches 35.4% at an ITO layer thickness of 1840 nm. Then, we can start the simulation again assuming $d = 978$ nm, $d_0 = 1840$ nm, $d_2 = 0.05d$, and $d_3 = 0.1d$ and solve for d_1, the thickness of the p-window confinement layer. The results indicate that the cell efficiency reaches 36.2% at an optimum window layer thickness of 210 nm. Repeating the process for d_3, the n-window confinement layer, the proposed cell efficiency increases to 36.7% when $d_3 = 98$ nm. The final step is the solution for d_2, the thickness of the 2D-GI index modulation layer. This process reveals the best enhancement of the proposed cell efficiency, reaching the optimum value of 39.2% at $d_2 = 52$ nm, as shown in Fig. 6. In addition, Fig. 6 shows that below and above the optimum layer thicknesses, the cell efficiency is degraded, except for the optimum thickness of the ITO-ARC layer, where the cell efficiency remains constant.

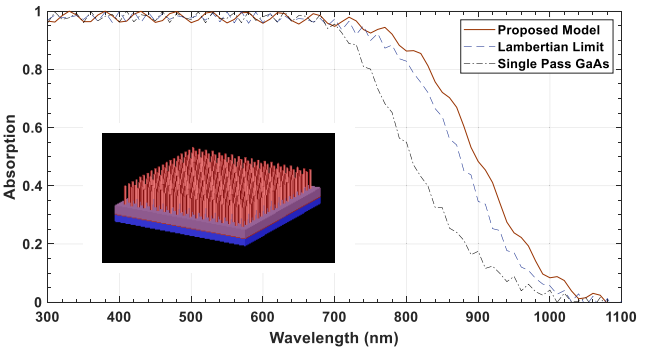

FIGURE 7. Proposed cell absorption compared with single-pass absorption and Lambertian limit versus the wavelength; d = 978 nm and the shadow coupling efficiencies product $\eta_s \eta_c = 6.6\%$.

IV. RESULTS AND DISCUSSIONS

Using the optimum parameter results in the previous section, we calculated the proposed cell absorption, efficiency, and electrical characteristics. Fig. 7 shows the proposed cell absorption compared with a single-photon pass through the planar cell structure and the Lambertian absorption limit considering the shadowing effect, coupling effect, and a quantum efficiency that is still unity. From 300 nm to 700 nm, all normalized absorptions are approximately the same; at wavelengths greater than 700 nm, the proposed cell absorption outperforms the other absorptions because of the perfect impedance matching between layers resulting from using the PhC light-trapping layer structures. Considering this result, we can use Eq. (5) to calculate the absorption enhancement factor, $F(\lambda)$.

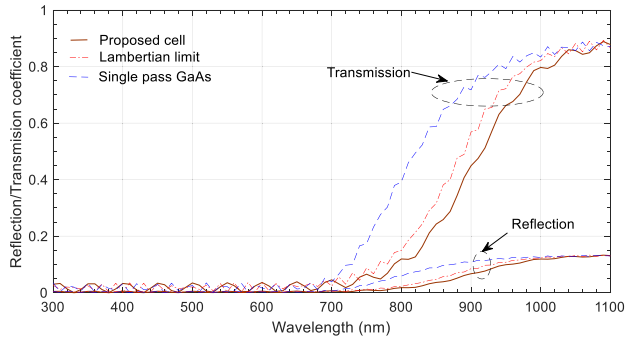

FIGURE 8. Proposed cell reflection and transmission coefficients compared with single-pass absorption and Lambertian limit versus the wavelength; d = 978 nm and the shadow coupling efficiencies product $\eta_s\eta_c = 6.6\%$.

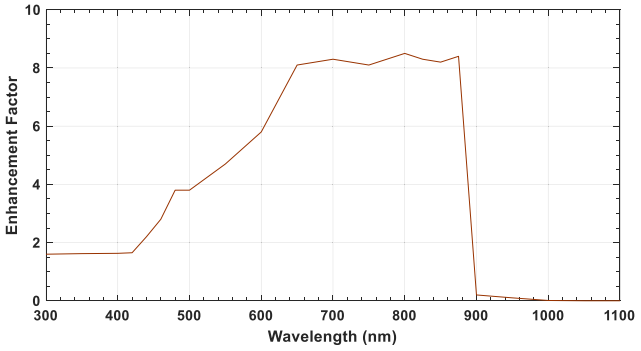

FIGURE 9. Enhancement factor of proposed cell structure.

Reflection/transmission coefficients for the proposed cell structure compared with the single-pass GaAs cell and Lambertian limit of the same 978 nm active layer thickness are shown in Fig. 8. From the figure, one can observe that above 700 nm the proposed cell has low reflection and transmission due to better index matching between layers provided by the index modulation layers. In the ultraviolet and visible regions, the reflection/transmission coefficients of the proposed cell, single-pass cell, and Lambertian limit are the same and very low. Overall, the absorption of the proposed cell is better than the others due to increasing the diffraction of photons within the active layer provided by the index modulation layer ITO trapping layer.

Figure 9 demonstrates the absorption enhancement factor; the results show that the enhancement factor is approximately 1.5 from 300 nm to 425 nm. At wavelengths greater than 425 nm, the factor increased to 8.2, starting from 650 nm to 880 nm, and the cell efficiency enhancement factor is 145% compared with the single-pass absorption and efficiency, respectively. In the aforementioned range, the light-trapping structure is responsible for coupling, guiding, and deflecting the incident photons for absorption inside the modified active layer with the 2D-GI index modulation.

The number of electron hole pairs combined at a certain wavelength λ and collected at the cell electrodes can be

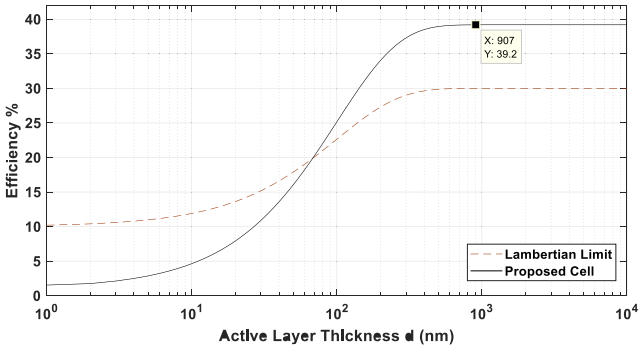

FIGURE 10. Proposed cell efficiency compared with the Lambertian efficiency limit.

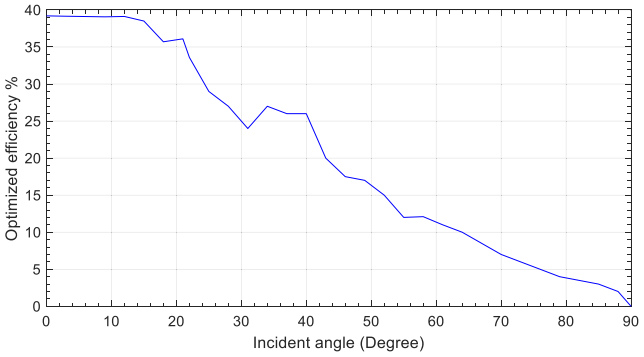

FIGURE 11. Proposed cell efficiency versus the incident angle.

expressed as [1]:

$$n_{e-h}(\lambda) = \frac{\lambda}{hC} \sum_i \eta_s \eta_c I(\lambda) A_i(\lambda) \tag{7}$$

where h is Planck's constant and C is the free space speed of light. Integrating Eq. (7) over the wavelength range from 300 to 1100 nm, we can obtain the total number of electron–hole pairs that are collected by the cell electrodes, as in Eq. (8).

$$N_{e-h} = \int_{300nm}^{1100nm} n_{e-h}(\lambda)\, d\lambda \tag{8}$$

During the simulation, the incremental step $\Delta\lambda$ was 0.5 nm, using the previous equation and with no absorption above the GaAs energy band gap value of 1.432 eV. The short-circuit current density J_{sc} can be simply calculated from Eq. (9) as:

$$J_{sc} = qN_{e-h} \tag{9}$$

where, q is the electron charge. Additionally, the proposed cell open-circuit voltage V_{oc} can be expressed as:

$$V_{oc} = \frac{KT}{q} \ln\left(\frac{J_{sc}}{J_{so}} + 1\right) \tag{10}$$

Assume $T = 298^0$K, K is Boltzmann's constant, and J_{so} is the cell junction reverse saturation current. Considering

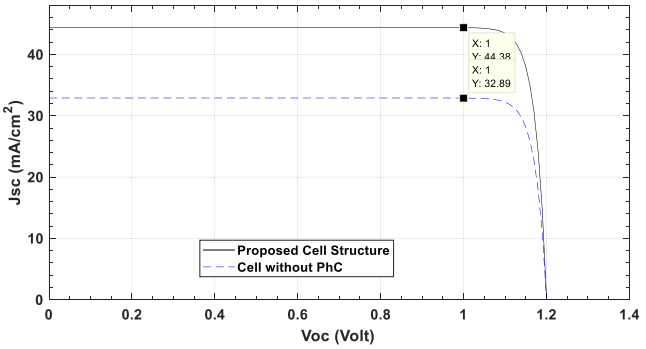

FIGURE 12. Proposed cell short circuit current density versus open circuit voltage compared with the planar cell electrical characteristics when $\eta = 39.2\%$ and $d = 907$ nm.

Eq. (9) and Eq. (10), the maximum conversion efficiency of the proposed cell can be rewritten as:

$$\eta = \frac{FFV_{oc}J_{sc}}{P_{in}} \tag{11}$$

where, $P_{in} = \int I(\lambda)\, d\lambda$ is the incident optical power and F is the cell filling factor, which is represented by (12) as:

$$FF = \frac{V_m J_m}{V_{oc} J_{sc}} \tag{12}$$

where, $V_m J_m$ is the voltage current density product that represents the maximum power point of the cell. Fig. 10 illustrates the proposed cell conversion efficiency curve compared with the Lambertian efficiency limit as a function of the active layer thickness considering all the optimum parameters calculated in this study. This graph indicates that when the active layer thickness exceeds 70 nm, the proposed cell structure with the PhC layers outperforms the Lambertian efficiency limit. In addition, when the active layer thickness reaches 907 nm, including the 104-nm thicknesses of the GI layers, the proposed cell efficiency reaches the optimum value of 39.2%. This figure also shows that it is possible to design a 70-nm GaAs nano solar cell with an efficiency of 17.5%, which is better than that of the same thickness using Lambertian efficiency conditions.

Figure 11 demonstrates the variation in the proposed cell efficiency versus the incident angle. The result indicates that when the incident angle increases, the efficiency of the proposed cell decrease. Additionally, within the incident range from 0^0 to 40^0, the proposed cell is less sensitive to the incident light, and the cell efficiency decreased by 36% only. For the solar cells based on the 2D-PhC structures, the absorption can be controlled by the Bloch modes that correspond to the almost flat photonic bands.

Then the weak variation of its characteristics with the incidence angle explains the lower decrease of the PhC based structure global efficiency. In addition, the minimum drops in cell efficiency and then increase at the minimum tilted incident angle are due to two reasons. First, the zeroth-order reflection path length can slightly increase by the tilted incidence angle; second, the first-order reflections

TABLE 1. FDTD simulation parameters.

FDTD setting	General	Dimension		3D
		Background index		1
		Sampling time (fs)		1000
	Geometry	X-Span		10 µm
		Y-Span		10 µm
		Z-Span		Different layers
	Mesh setting	Step Time	stability factor	0.99
			dt(fs)	0.069
		Mesh step size		25 nm
	Boundary conditions			Z-metal, X and Y periodic and symmetric
Source setting	General	Source shape		Plane wave
		Normalized amplitude		1
		Phase		0 and variable
	Geometry	X-Span		10 µm
		Y-Span		10 µm
		Z-Span		1µm, 50 nm
	Wavelength	Start		0.3 µm
		End		1.1 µm

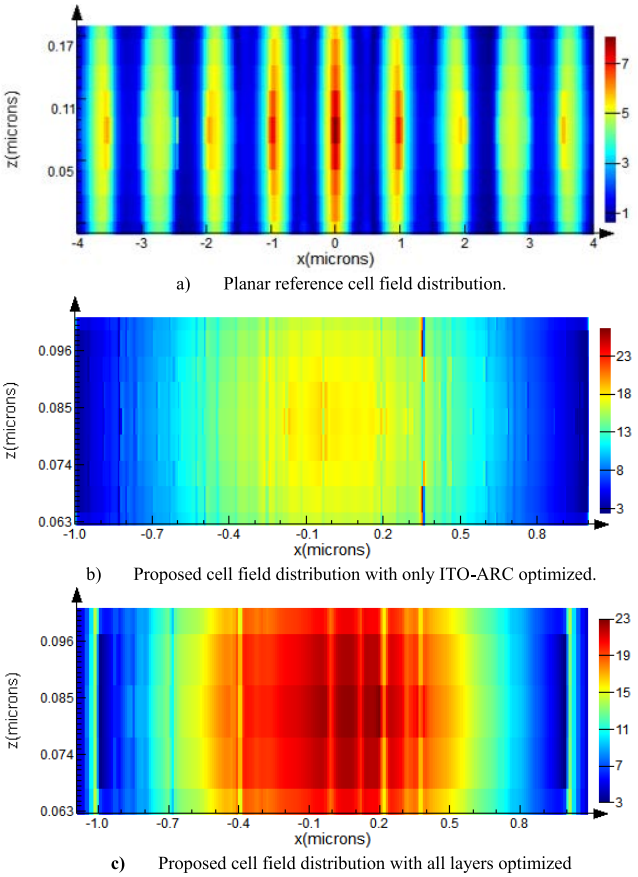

FIGURE 13. Cell electric field distribution within 50 nm of the center of the active layer in the range 300–1100 nm: a) planar reference cell, b) proposed cell with ITO layer optimization only, and c) proposed cell with all layers optimized.

can be broken by the tilted incidence, same as in the blazed grating case. The proposed cell short-circuit current density

TABLE 2. Summary of the optimal parameters through optimization steps.

No.	Optimization Step	Parameters	Values (nm)	Cell efficiency
1	Design the ITO-ARC Trapping Layer	Active layer thickness including the thicknesses of GI layers d	1000	**33.7%**
2		ITO structure lattice constant a	**500**	
3		ITO structure nanorod diameters D	**190**	
4		ITO structure layer thickness d_0	2000	
5		D/a ratio	0.38	
6		Front window confinement layer p-Al(0.85)GaAs d_1	200	
7		Back window confinement layer n-Al(0.35)GaAs d_3	100	
8		2D-GI modulation index layer thickness d_2	50	
9		Al back electrode thickness	800	
1	Optimize the ITO-ARC Trapping Layer	Active layer thickness including the thicknesses of GI layers d	**978**	**35.4%**
2		ITO structure lattice constant a	500	
3		ITO structure nanorod diameters D	190	
4		ITO structure layer thickness d_0	**1840**	
5		D/a ratio	0.38	
6		Front window confinement layer p-Al(0.85)GaAs d_1	200	
7		Back window confinement layer n-Al(0.35)GaAs d_3	100	
8		2D-GI modulation index layer thickness d_2	50	
9		Al back electrode thickness	800	
1	Optimize the Window Confinement Layers	Active layer thickness including the thicknesses of GI layers d	978	**36.7%**
2		ITO structure lattice constant a	500	
3		ITO structure nanorod diameters D	190	
4		ITO structure layer thickness d_0	1840	
5		D/a ratio	0.38	
6		Front window confinement layer p-Al(0.85)GaAs d_1	**210**	
7		Back window confinement layer n-Al(0.35)GaAs d_3	**98**	
8		2D-GI modulation index layer thickness d_2	50	
9		Al back electrode thickness	800	
1	Optimize the 2D-GI Index Modulation Layers	Active layer thickness including the thicknesses of GI layers d	**907**	**39.2%**
2		ITO structure lattice constant a	500	
3		ITO structure nanorod diameters D	190	
4		ITO structure layer thickness d_0	1840	
5		D/a ratio	0.38	
6		Front window confinement layer p-Al(0.85)GaAs d_1	210	
7		Back window confinement layer n-Al(0.35)GaAs d_3	98	
8		2D-GI modulation index layer thickness d_2	**52**	
9		Al back electrode thickness	800	

versus open-circuit voltage is illustrated in Fig. 12. In this calculation, the parasitic absorption loss at the interface between the n-Al(0.35)GaAs dielectric layer and the Al back electrode is considered. The use of the 2D-GI index modulation layer reduces this parasitic loss compared with the planar cell PhC-free structure. This enhances the proposed cell short-circuit current compared with the planar cell structure by a factor of 1.35 at an open-circuit voltage of 1 V, as shown in Fig. 12. The proposed cell structure can produce a short-circuit current of 44.38 mA/cm^2 at a 1-V open-circuit voltage, which is a good cell characteristic compared with the results in the literature.

The difficulty of fabricating the ITO nanostructure on the GaAs nanostructure represented the layered ARCs to satisfy the requirement of omnidirectional antireflection and broadband [85]. Table 1 presents the simulation parameters of the proposed cell structure. These parameters are classified into source settings and FDTD settings when the boundary conditions are set to metal in z-direction and periodic-symmetry in x-y directions. Therefore, all settings are adjusted to conduct the simulation in a wavelength range from 300 –1100 nm.

Figure 13 illustrates the electric field intensity within 50 nm of the z-axis center of the active layer in the wavelength range from 300 nm to 1100 nm. Fig. 13-a represents the field intensity of the planar cell without any Trapping structure. Whereas Fig. 13-b represents the field distribution of the proposed cell when only the ITO-ARC layer thickness is optimized, and Fig. 13-c represents the field distribution of the proposed cell when the thickness of all layers is optimized. The results of field distributions in Fig. 13-b and Fig. 13 are focused on 2 μm around the x-axis center. The results show that the electric field intensity of the fully optimized cell is improved by a factor of 3.285 compared with the planar cell and 1.278 compared with the proposed ITO-layer optimization only. This is due to the enhancement of carrier confinement and the photocurrent in the fully optimized cell. In these results, the simulations conducted in the wavelength range from 300 nm to 1100 nm, and the incident light is normal to the cell front surface.

Table 2 Summarize the optimum dimensions and efficiency of the proposed cell. The bold values are the current optimized values in each step during the optimization process. Fig. 14 shows the electric field intensities of the

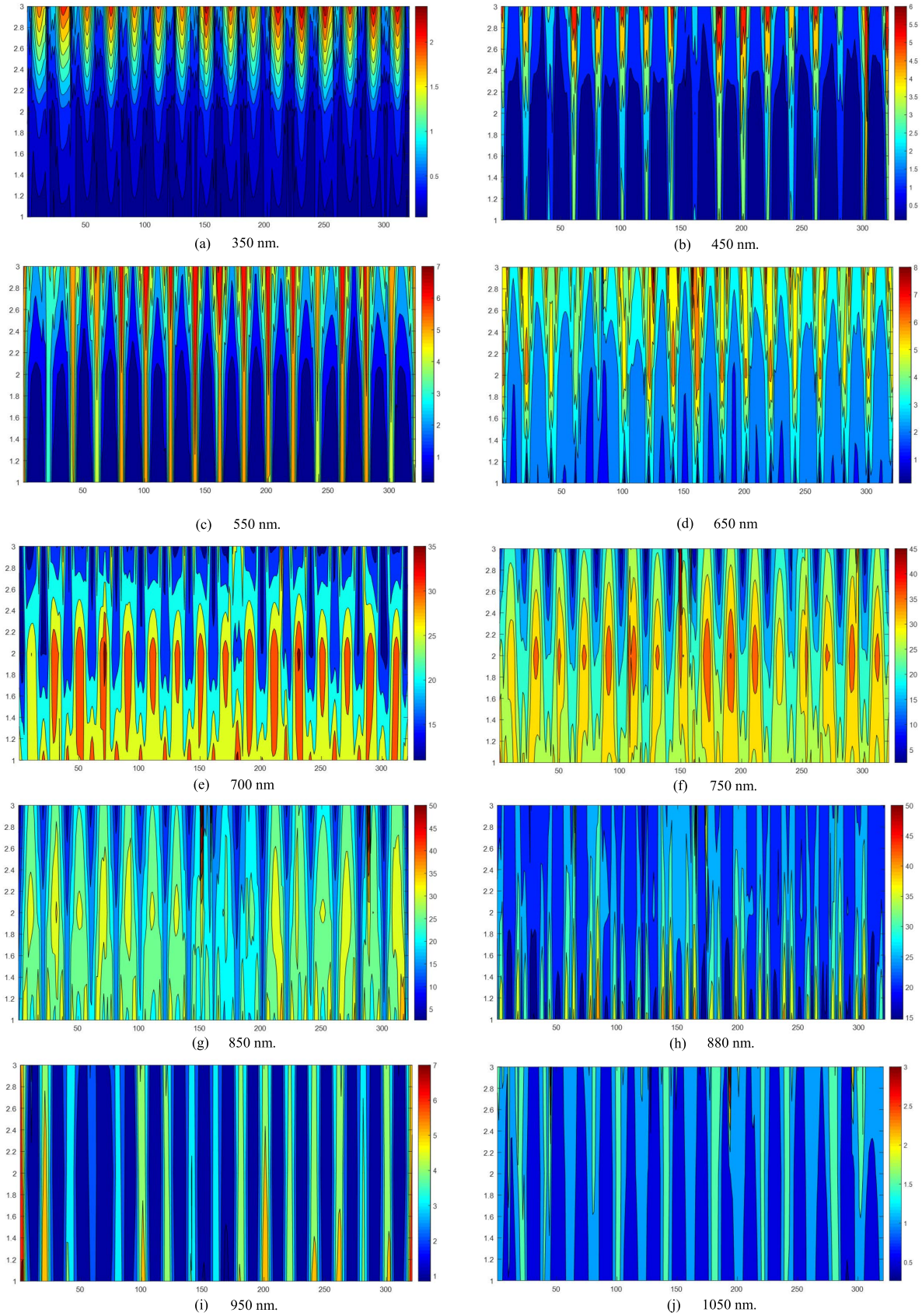

FIGURE 14. Proposed cell electric field distribution within 50 nm of the center of the active layer at wavelengths of a) 350 nm, b) 450 nm C) 550 nm, d) 650 nm, e) 700 nm, f) 750 nm, g) 850 nm, h) 880 nm, i) 950 nm, and j) 1050 nm.

proposed cell at ten different wavelengths from 350 nm to 1050 nm within 50 nm of the z-axis center of the active layer and 8 μm of the x-axis center. These figures illustrate that the optimum wavelength range for absorption started from 550 nm to 880 nm, as shown in Fig.14-c–Fig.14-h. These results confirm that shown in Fig.9. From 350 nm to 450 nm, the wavelengths of higher photon energy and the electric field intensity of the proposed structure in this range are improved by a factor of 2.25 compared with the field intensity results from the planar cell. The coupling of light from 880 nm to 1100 nm has been reduced compared with that in the range from 550 nm to 880 nm, which is due to the reduction in the photon energy at higher wavelengths. The results shown in Fig. 14-i and Fig. 14-j prove the extension in the absorption range of the proposed cell. This extension is due to the modification in the bandgap of the proposed cell by the added index modulation layers.

The index modulation layers make a smooth continuity in the band diagram around the active layer edges. Finally, the proposed structure provides high field intensity in the wavelength range from 550 nm to 880 nm below this range, from 350 nm to 500 nm, the enhancement is approximate twice the field intensity provided by the planar cell, and above this range, from 880 nm to 1050 nm, the field intensity provided by the proposed structure is low, but this not occurs in the planar cell because the index modulation layers do not exist.

V. CONCLUSION

In this paper, an improved optical design of a nano solar cell is presented based on a 900-nm thin GaAs active layer with a 2D-PhC light trapping ITO-ARC structure at the top, with the help of an Al back reflector electrode layer to collect the electrons. In addition, for further improvement, a 2D-PhC structure working as a 2D-GI index modulation layer was added in contact with the active layer to increase the photocurrent, achieving an efficiency of 39.2% and a short-circuit electric current of 44.38 mA/cm^2. The results showed a significant improvement in the absorption through the photovoltaic spectra of solar cells. The results were compared with the Lambertian limit and compared with the results of a GaAs planar solar cell with the same active layer thickness. These results show an absorption of up to eight times that of the planar cell in the light spectrum from 650 to 880 nm. The results also proved that the proposed cell efficiency was enhanced by 45 percent and 31 percent compared with those of the planar cell and Lambertian limit, respectively. The added layers confine the low-energy photons inside the active layer and increase the light spectrum of the cell to 1050 nm. Finally, it is notable that the improved cell can be manufactured at a low cost.

REFERENCES

[1] N. D. Gupta and V. Janyani, "Lambertian and photonic light trapping analysis with thickness for GaAs solar cells based on 2D periodic pattern," *IET Optoelectron.*, vol. 11, no. 5, pp. 217–224, Sep. 2017, doi: 10.1049/iet-opt.2017.0002.

[2] N. D. Gupta and V. Janyani, "Design and analysis of light trapping in thin film GaAs solar cells using 2-D photonic crystal structures at front surface," *IEEE J. Quantum Electron.*, vol. 53, no. 2, pp. 1–9, Apr. 2017, doi: 10.1109/JQE.2017.2667638.

[3] N. D. Gupta, V. Janyani, and M. Mathew, "Light trapping in p-i-n superlattice based InGaN/GaN solar cells using photonic crystal," *Opt. Quantum Electron.*, vol. 48, no. 11, p. 502, Nov. 2016, doi: 10.1007/s11082-016-0775-8.

[4] N. D. Gupta, "Absorption enhancement in hole interface layer free perovskite solar cells using periodic photonic nanostructures," *Opt. Laser Technol.*, vol. 115, pp. 20–31, Jul. 2019, doi: 10.1016/j.optlastec.2019.01.052.

[5] N. D. Gupta, "Comparison of light trapping limits derived using various methods for thin film GaAs solar cells," *J. Nanosci. Nanotechnol.*, vol. 20, no. 6, pp. 3939–3942, Jun. 2020, doi: 10.1166/jnn.2020.17504.

[6] N. D. Gupta and V. Janyani, "Design and optimization of photonic crystal diffraction grating based efficient light trapping structure for GaAs thin film solar cell," *J. Nanoelectron. Optoelectron.*, vol. 11, no. 4, pp. 407–415, Aug. 2016.

[7] A. Zhang and Z. Guo, "Efficient light trapping in tapered silicon nanohole arrays," *Optik*, vol. 127, no. 5, pp. 2861–2865, Mar. 2016, doi: 10.1016/j.ijleo.2015.12.001.

[8] G. Dai, R. Wu, A. Zhang, X. Bao, H. Zhou, F. Shen, and Z. Guo, "Light trapping performance of the silicon nanowire and nanocone based solar cells," *J. Optoelectron. Adv. Mater.*, vol. 18, nos. 7–8, pp. 618–624, 2016.

[9] A. Zhang, Z. Guo, Y. Tao, W. Wang, X. Mao, G. Fan, K. Zhou, and S. Qu, "Advanced light-trapping effect of thin-film solar cell with dual photonic crystals," *Nanosc. Res. Lett.*, vol. 10, no. 1, pp. 1–10, Dec. 2015, doi: 10.1186/s11671-015-0912-5.

[10] K. Zhou, Z. Guo, S. Liu, and J.-H. Lee, "Current approach in surface plasmons for thin film and wire array solar cell applications," *Materials*, vol. 8, no. 7, pp. 4565–4581, Jul. 2015, doi: 10.3390/ma8074565.

[11] R. R. Das, S. Maity, A. Chowdhury, and A. Chakraborty, "RF/Analog performance of GaAs multi-fin FinFET with stress effect," *Microelectron. J.*, vol. 117, Nov. 2021, Art. no. 105267, doi: 10.1016/j.mejo.2021.105267.

[12] A. K. Dikshit, S. Maity, N. Mukherjee, and P. Chakrabarti, "Hybrid inorganic–organic inverted solar cells with ZnO/ZnMgO barrier layer and effective organic active layer for low leakage current, enhanced efficiency, and reliability," *IEEE J. Photovolt.*, vol. 11, no. 4, pp. 983–990, Jul. 2021, doi: 10.1109/JPHOTOV.2021.3067828.

[13] S. Maity, B. Das, R. Maity, N. P. Maity, K. Guha, and K. S. Rao, "Improvement of quantum and power conversion efficiency through electron transport layer modification of ZnO/perovskite/PEDOT: PSS based organic heterojunction solar cell," *Sol. Energy*, vol. 185, pp. 439–444, Jun. 2019, doi: 10.1016/j.solener.2019.04.092.

[14] S. Maity and T. Thomas, "Hole-collecting treated graphene layer and PTB7: PC71BM-based bulk-heterojunction OPV with improved carrier collection and photovoltaic efficiency," *IEEE Trans. Electron Devices*, vol. 65, no. 10, pp. 4548–4554, Oct. 2018, doi: 10.1109/TED.2018.2864537.

[15] A. Richter, M. Hermle, and S. W. Glunz, "Reassessment of the limiting efficiency for crystalline silicon solar cells," *IEEE J. Photovolt.*, vol. 3, no. 4, pp. 1184–1191, Oct. 2013.

[16] A. Mavrokefalos, S. E. Han, S. Yerci, M. S. Branham, and G. Chen, "Efficient light trapping in inverted nanopyramid thin crystalline silicon membranes for solar cell applications," *Nano Lett.*, vol. 12, no. 6, pp. 2792–2796, Jun. 2012.

[17] K. Yoshikawa, H. Kawasaki, W. Yoshida, T. Irie, K. Konishi, K. Nakano, T. Uto, D. Adachi, M. Kanematsu, H. Uzu, and K. Yamamoto, "Silicon heterojunction solar cell with interdigitated back contacts for a photoconversion efficiency over 26%," *Nature Energy*, vol. 2, no. 5, pp. 1–8, May 2017.

[18] A. Chutinan and S. John, "Light trapping and absorption optimization in certain thin-film photonic crystal architectures," *Phys. Rev. A, Gen. Phys.*, vol. 78, no. 2, Aug. 2008, Art. no. 023825.

[19] G. Demésy and S. John, "Solar energy trapping with modulated silicon nanowire photonic crystals," *J. Appl. Phys.*, vol. 112, no. 7, Oct. 2012, Art. no. 074326.

[20] A. Deinega and S. John, "Solar power conversion efficiency in modulated silicon nanowire photonic crystals," *J. Appl. Phys.*, vol. 112, no. 7, Oct. 2012, Art. no. 074327.

[21] S. Eyderman, S. John, and A. Deinega, "Solar light trapping in slanted conical-pore photonic crystals: Beyond statistical ray trapping," *J. Appl. Phys.*, vol. 113, no. 15, Apr. 2013, Art. no. 154315.

[22] S. Eyderman, S. John, M. Hafez, S. S. Al-Ameer, T. S. Al-Harby, Y. Al-Hadeethi, and D. M. Bouwes, "Light-trapping optimization in wet-etched silicon photonic crystal solar cells," *J. Appl. Phys.*, vol. 118, no. 2, Jul. 2015, Art. no. 023103.

[23] A. S. M. Mohsin, M. Mobashera, A. Malik, M. Rubaiat, and M. Islam, "Light trapping in thin-film solar cell to enhance the absorption efficiency using FDTD simulation," *J. Opt.*, vol. 49, no. 4, pp. 523–532, Dec. 2020, doi: 10.1007/s12596-020-00656-w.

[24] M. S. Branham, W. Hsu, S. Yerci, J. Loomis, S. V. Boriskina, B. R. Hoard, S. E. Han, and G. Chen, "15.7% efficient 10-μm-thick crystalline silicon solar cells using periodic nanostructures," *Adv. Mater.*, vol. 27, no. 13, pp. 2182–2188, 2015.

[25] K. Kumar, A. Khalatpour, G. Liu, J. Nogami, and N. P. Kherani, "Converging photo-absorption limit in periodically textured ultra-thin silicon foils and wafers," *Sol. Energy*, vol. 155, pp. 1306–1312, Oct. 2017.

[26] M. Ernst and R. Brendel, "Lambertian light trapping in thin macroporous silicon layers," *Phys. Status Solidi RRL*, vol. 8, pp. 1–3, Dec. 2014.

[27] A. Bozzola, M. Liscidini, and L. C. Andreani, "Photonic light-trapping versus Lambertian limits in thin film silicon solar cells with 1D and 2D periodic patterns," *Opt. Exp.*, vol. 20, no. S2, p. A224, Mar. 2012.

[28] M. F. Schumann, M. Langenhorst, M. Smeets, K. Ding, U. W. Paetzold, and M. Wegener, "All-angle invisibility cloaking of contact fingers on solar cells by refractive free-form surfaces," *Adv. Opt. Mater.*, vol. 5, no. 17, Sep. 2017, Art. no. 1700164.

[29] P. Campbell and M. A. Green, "Light trapping properties of pyramidally textured surfaces," *J. Appl. Phys.*, vol. 62, no. 1, pp. 243–249, Jul. 1987.

[30] I. Valuev, A. Deinega, A. Knizhnik, and B. Potapkin, "Creating numerically efficient FDTD simulations using generic C++ programming," in *Computational Science and Its Applications* (Lecture Notes in Computer Science), vol. 4707, O. Gervasi, M. L. Gavrilova, Eds. Berlin, Germany: Springer, 2007, pp. 213–226, doi: 10.1007/978-3-540-74484-9_19.

[31] J. Zhao and A. Wang, "Rear emitter n-type passivated emitter, rear totally diffused silicon solar cell structure," *Appl. Phys. Lett.*, vol. 88, no. 24, Jun. 2006, Art. no. 242102.

[32] M. F. Schumann, M. Langenhorst, M. Smeets, K. Ding, U. W. Paetzold, and M. Wegener, "All-angle invisibility cloaking of contact fingers on solar cells by refractive free-form surfaces," *Adv. Opt. Mater.*, vol. 5, no. 17, Sep. 2017, Art. no. 1700164.

[33] J. Zhao, A. Wang, P. Campbell, and M. A. Green, "22.7% efficient silicon photovoltaic modules with textured front surface," *IEEE Trans. Electron Devices*, vol. 46, no. 7, pp. 1495–1497, Jul. 1999.

[34] M. F. Abdullah, M. A. Alghoul, H. Naser, N. Asim, S. Ahmadi, B. Yatim, and K. Sopian, "Research and development efforts on texturization to reduce the optical losses at front surface of silicon solar cell," *Renew. Sustain. Energy Rev.*, vol. 66, pp. 380–398, Dec. 2016.

[35] O. Höhn, N. Tucher, and B. Bläsi, "Theoretical study of pyramid sizes and scattering effects in silicon photovoltaic module stacks," *Opt. Exp.*, vol. 26, no. 6, p. A320, Mar. 2018.

[36] C. Schinke, P. C. Peest, J. Schmidt, R. Brendel, K. Bothe, M. R. Vogt, I. Kröger, S. Winter, A. Schirmacher, S. Lim, H. T. Nguyen, and D. MacDonald, "Uncertainty analysis for the coefficient of band-to-band absorption of crystalline silicon," *AIP Adv.*, vol. 5, no. 6, Jun. 2015, Art. no. 067168.

[37] S. Bhattacharya, I. Baydoun, M. Lin, and S. John, "Towards 30% power conversion efficiency in thin-silicon photonic-crystal solar cells," *Phys. Rev. A, Gen. Phys.*, vol. 11, no. 1, Jan. 2019, Art. no. 014005.

[38] D. H. Choi, S. K. Nam, K. Jung, and J. H. Moon, "2D photonic crystal nanodisk array as electron transport layer for highly efficient perovskite solar cells," *Nano Energy*, vol. 56, pp. 365–372, Feb. 2019, doi: 10.1016/j.nanoen.2018.11.050.

[39] M. Taguchi, A. Yano, S. Tohoda, K. Matsuyama, Y. Nakamura, T. Nishiwaki, K. Fujita, and E. Maruyama, "24.7% record efficiency HIT solar cell on thin silicon wafer," *IEEE J. Photovolt.*, vol. 4, no. 1, pp. 96–99, Jan. 2014.

[40] S. Guha, J. Yang, and B. Yan, "High efficiency multi-junction thin film silicon cells incorporating nanocrystalline silicon," *Sol. Energy Mater. Sol. Cells*, vol. 119, pp. 1–11, Dec. 2013.

[41] S. A. Boden and D. M. Bagnall, "Optimization of moth-eye antireflection schemes for silicon solar cells," *Prog. Photovoltaics: Res. Appl.*, vol. 18, no. 3, pp. 195–203, May 2010.

[42] Y. Kanamori, K. Hane, H. Sai, and H. Yugami, "100 nm period silicon antireflection structures fabricated using a porous alumina membrane mask," *Appl. Phys. Lett.*, vol. 78, no. 2, pp. 142–143, Jan. 2001.

[43] S. C-H, H. BJ, B. Jiang, and P. Jiang, "Biomimetic subwavelength antireflective gratings on GaAs," *Opt. Lett.*, vol. 33, no. 9, pp. 2224–2226, 2008.

[44] H. Sai, K. Saito, N. Hozuki, and M. Kondo, "Relationship between the cell thickness and the optimum period of textured back reflectors in thin-film microcrystalline silicon solar cells," *Appl. Phys. Lett.* vol. 102, no. 5, Feb. 2013, Art. no. 053509.

[45] C. Ulbrich, A. Gerber, K. Hermans, A. Lambertz, and W. Rau, "Analysis of short circuit current gains by an antireflective textured cover on silicon thin film solar cells," *Prog. Photovolt., Res. Appl.*, vol. 21, no. 8, pp. 1672–1681, 2013.

[46] H. Sai, T. Koida, T. Matsui, I. Yoshida, K. Saito, and M. Kondo, "Micro-crystalline silicon solar cells with 10.5% efficiency realized by improved photon absorption via periodic textures and highly transparent conductive oxide," *Appl. Phys. Exp.*, vol. 6, no. 10, Sep. 2013, Art. no. 104101.

[47] S. Chattopadhyay, Y. F. Huang, Y. J. Jen, A. Ganguly, K. H. Chen, and L. C. Chen, "Anti-reflecting and photonic nanostructures," *Mater. Sci. Eng., R, Rep.*, vol. 69, nos. 1–3, pp. 1–35, Jun. 2010.

[48] Y. M. Song, Y. Jeong, C. I. Yeo, and Y. T. Lee, "Enhanced power generation in concentrated photovoltaics using broadband antireflective coverglasses with moth eye structures," *Opt. Exp.*, vol. 20, no. S6, p. A916, 2012.

[49] W. Xu, B. Peng, J. Chen, M. Liang, and F. Cai, "New triphenylamine-based dyes for dye-sensitized solar cells," *J. Phys. Chem. C*, vol. 112, no. 3, pp. 874–880, Jan. 2008.

[50] P. Qin, X. Yang, R. Chen, L. Sun, T. Marinado, T. Edvinsson, G. Boschloo, and A. Hagfeldt, "Influence of-conjugation units in organic dyes for dye-sensitized solar cells," *J. Phys. Chem. C*, vol. 111, no. 4 pp. 1853–1860, 2007.

[51] S. H. Kang, J.-Y. Kim, Y. Kim, H. S. Kim, and Y.-E. Sung, "Surface modification of stretched TiO_2 nanotubes for solid-state dye-sensitized solar cells," *J. Phys. Chem. C*, vol. 111, no. 26, pp. 9614–9623, Jul. 2007.

[52] S. Eu, S. Hayashi, T. Umeyama, Y. Matano, Y. Araki, and H. Imahori, "Quinoxaline-fused porphyrins for dye-sensitized solar cells," *J. Phys. Chem. C*, vol. 112, no. 11, pp. 4396–4405, Mar. 2008.

[53] A. Morandeira, J. Fortage, T. Edvinsson, P. L. Le, E. Blart, G. Boschloo, A. Hagfeldt, L. Hanmiarstrom, and L. Dobel, "Improved photon-to-current conversion efficiency with a nanoporous P-type NiO electrode by the use of a sensitizer-acceptor dyad," *J. Phys. Chem. C*, vol. 112, pp. 1721–1728, Feb. 2008.

[54] Y. Cao, Y. Bai, Q. Yu, Y. Cheng, S. Liu, D. Shi, F. Gao, and P. Wang, "Dye-sensitized solar cells with a high absorptivity ruthenium sensitizer featuring a 2-(Hexylthio)thiophene conjugated bipyridine," *J. Phys. Chem. C*, vol. 113, no. 15, pp. 6290–6297, Apr. 2009.

[55] S. Colodrero, A. Mihi, J. A. Anta, M. Ocaña, and H. Míguez, "Experimental demonstration of the mechanism of light harvesting enhancement in photonic-crystal-based dye-sensitized solar cells," *J. Phys. Chem. C*, vol. 113, no. 4, pp. 1150–1154, Jan. 2009.

[56] P. R. F. Barnes, A. Y. Anderson, S. E. Koops, J. R. Durrant, and B. C. O'Regan, "Electron injection efficiency and diffusion length in dye-sensitized solar cells derived from incident photon conversion efficiency measurements," *J. Phys. Chem. C*, vol. 113, no. 3, pp. 1126–1136, Dec. 2009.

[57] M. D. Brown, T. Suteewong, R. S. S. Kumar, V. D'Innocenzo, A. Petrozza, M. M. Lee, U. Wiesner, and H. J. Snaith, "Plasmonic dye-sensitized solar cells using core-shell metal-insulator nanoparticles," *Nano Lett.*, vol. 11, no. 2, pp. 438–445, Feb. 2011.

[58] N. Memarian, I. Concina, A. Braga, S. M. Rozati, A. Vomiero, and G. Sberveglieri, "Hierarchically assembled ZnO nanocrystallites for high-efficiency dye-sensitized solar cells," *Angewandte Chemie*, vol. 50, pp. 12321–12325, Dec. 2011.

[59] M. McCune, W. Zhang, and Y. Deng, "High efficiency dye-sensitized solar cells based on three-dimensional multilayered ZnO nanowire arrays with 'caterpillar-like' structure," *Nano Lett.*, vol. 12, no. 7, pp. 3656–3662, Jul. 2012.

[60] N. Yamanaka, R. Kawano, W. Kubo, N. Masaki, T. Kitamura, Y. Wada, M. Watanabe, and S. Yanagida, "Dye-sensitized TiO_2 solar cells using imidazolium-type ionic liquid crystal systems as effective electrolytes," *J. Phys. Chem. B*, vol. 111, no. 18, pp. 4763–4769, May 2007.

[61] F. Fabregat-Santiago, J. Bisquert, E. Palomares, L. Otero, D. Kuang, S. M. Zakeeruddin, and M. Grätzel, "Correlation between photovoltaic performance and impedance spectroscopy of dye-sensitized solar cells based on ionic liquids," *J. Phys. Chem. C*, vol. 111, pp. 6550–8560, May 2007.

[62] H. A. Atwater and A. Polman, "Plasmonics for improved photovoltaic devices," *Nat. Mater.*, vol. 9, no. 3, pp. 205–213, Mar. 2010.

[63] A. J. Nozik, "Nanoscience and nanostructures for photovoltaics and solar fuels," *Nano Lett.*, vol. 10, no. 8, pp. 2735–2741, Aug. 2010.
[64] M. Graetzel, R. A. J. Janssen, D. B. Mitzi, and E. H. Sargent, "Materials interface engineering for solution-processed photovoltaics," *Nature*, vol. 488, no. 7411, pp. 304–312, Aug. 2012.
[65] T. Toyoda and Q. Shen, "Effect of nanostructured TiO_2 morphologies on photovoltaic properties," *J. Phys. Chem. Lett.*, vol. 3, pp. 1885–1893, 2012.
[66] M. Shalom, S. Buhbut, S. Tirosh, and A. Zaban, "Design rules for high-efficiency quantum-dot-sensitized solar cells: A multilayer approach," *J. Phys. Chem. Lett.*, vol. 3, no. 17, pp. 2436–2441, Sep. 2012.
[67] P. V. Kamat, "Quantum dot solar cells. The next big thing in photovoltaics," *J. Phys. Chem. Lett.*, vol. 4, pp. 908–918, Mar. 2013.
[68] W. A. Badawy, "Quantum dots and nano-porous materials for solar energy conversion," in *Fuelling the Future: Advances in Science and Technologies for Energy Generation, Transmission and Storage*, A. Mendez, Ed. Boca Raton, FL, USA: Brown Walker Press, 2012, pp. 235–242.
[69] V. Aroutiounian, S. Petrosyan, A. Khachatryan, and K. Touryan, "Quantum dot solar cells," *Proc. SPIE*, vol. 4458, pp. 2268–2271, Nov. 2001, doi: 10.1117/12.448264.
[70] A. J. Nozik, "Quantum dot solar cells," *Phys. E, Low-Dimensional Syst. Nanostruct.*, vol. 14, nos. 1–2, pp. 115–120, 2002.
[71] P. Yu, K. Zhu, A. G. Norman, S. Ferrere, A. J. Frank, and A. J. Nozik, "Nano-crystalline TiO_2 solar cells sensitized with InAs quantum dots," *J. Phys. Chem. B*, vol. 110, pp. 25451–25454, Dec. 2006.
[72] J.-Y. Chang, J.-M. Lin, L.-F. Su, and C.-F. Chang, "Improved performance of $CuInS_2$ quantum dot-sensitized solar cells based on a multilayered architecture," *ACS Appl. Mater. Interfaces*, vol. 5, no. 17, pp. 8740–8752, Sep. 2013, doi: 10.1021/am402547e.
[73] E. Puyoo, G. Rey, E. Appert, V. Consonni, and D. Bellet, "Efficient dye-sensitized solar cells made from ZnO nanostructure composites," *J. Phys. Chem. C*, vol. 116, no. 34, pp. 18117–18123, Aug. 2012.
[74] C. Xu, J. Wu, U. V. Desai, and D. Gao, "High-efficiency solid-state dye-sensitized solar cells based on TiO_2-coated ZnO nanowire arrays," *Nano Lett.*, vol. 12, no. 5, pp. 2420–2424, May 2012.
[75] A. Y. Mahmoud, J. Zhang, D. Ma, R. Izquierdo, and V.-V. Truong, "Thickness dependent enhanced efficiency of polymer solar cells with gold nanorods embedded in the photoactive layer," *Sol. Energy Mater. Sol. Cells*, vol. 116, pp. 1–8, Sep. 2013.
[76] P. V. Kamat, "Meeting the clean energy demand: Nanostructure architectures for solar energy conversion," *J. Phys. Chem. C*, vol. 111, no. 7, pp. 2834–2860, 2007.
[77] P. LM, "Characterization and modeling of dye-sensitized solar cells," *J. Phys. Chem. C*, vol. 111, pp. 6601–6612, May 2007.
[78] P. V. Kamat, "Quantum dot solar Cells. Semiconductor nanocrystals as light harvesters," *J. Phys. Chem. C*, vol. 112, no. 48, pp. 18737–18753, Dec. 2008.
[79] M. Shalom, S. Dor, S. Rühle, L. Grinis, and A. Zaban, "Core/CdS quantum dot/shell mesoporous solar cells with improved stability and efficiency using an amorphous TiO_2 coating," *J. Phys. Chem. C*, vol. 113, no. 9, pp. 3895–3898, Mar. 2009.
[80] W. J. Plieth, G. Pfuhl, A. Felske, and W. Badawy, "Photoetching of III/V semiconductors," *Electrochimica Acta*, vol. 34, no. 8, pp. 1133–1140, Aug. 1989.
[81] W. A. Badawy, G. Pfuhl, and W. J. Plieth, "ChemInform abstract: Electrochemical and photoelectrochemical behavior of n-GaAs and p-GaAs in the presence of H_2O_2," *ChemInform*, vol. 21, no. 19, pp. 531–537, May 1990.
[82] R. M. El-Sherif, S. A. Khalil, and W. A. Badawy, "Metal-assisted etching of p-silicon—Pore formation and characterization," *J. Alloys Compounds*, vol. 509, no. 10, pp. 4122–4126, Mar. 2011.
[83] M. A. Morsy and A. S. Alsayyari, "BER performance of OCDMA system based on optimised 2D PhC passive encoder," *IET Commun.*, vol. 14, no. 8, pp. 1268–1274, May 2020.
[84] (2004). N.R.E. Laboratory. *Reference Solar Spectral Irradiance: Air Mass 1.5 (G-173-03, ASTM)*. Accessed: Sep. 2016. [Online]. Available: http://rredc.nrel.gov/solar/spectra/am1.5/
[85] J. Cai and L. Qi, "Recent advances in antireflective surfaces based on nanostructure arrays," *Mater. Horizons*, vol. 2, pp. 37–53, Sep. 2015.

MORSY A. MORSY was born in Cairo, Egypt, in 1979. He received the B.Sc., M.Sc., and Ph.D. degrees from the Faculty of Engineering, Ain Shams University, Cairo, in 2000, 2007, and 2013, respectively. He is currently an Associate Professor of analog and digital communication, wave propagation and antennas, photonics, optical fiber communication systems, optical code division multiple access (OCDMA) networks, coding and performance analysis, and microwave devices with the Electrical Engineering Department, College of Engineering, Shaqra University, Ar. Riyadh, Saudi Arabia. He was a member of the ABET and NCAAA teams and published 17 journals and four conference papers. His research interests include optical communications, free space optics, visible light communications, photonics, 2D-photonic crystals, RF energy harvesting systems, optical communication networks, finite difference time domain (FDTD) analysis, and nano optical devices.

KHALID SALEH received the bachelor's degree in electrical engineering from King Saud University, Riyadh, Saudi Arabia, in 2006, the master's degree in electrical engineering from the University of Colorado, Denver, CO, USA, in 2010, and the Ph.D. degree from Arizona State University, Tempe, AZ, USA, in 2017. He has taught various courses like automatic control systems, digital control systems, and electric circuits. He is currently the Dean of the College of Engineering, Shaqra University, Al Duwadimi, Saudi Arabia. His research interests include applied mathematics, fractional order systems, signals analysis, digital image processing, linear and nonlinear systems analysis, and digital control systems.